



Lithological Discrimination of Parts of the Bhukia Area, Banswara District, Rajasthan Using Hyperspectral Data

Ashutosh Rohta¹ · Richa Upadhyay Sharma¹ · Shovan L. Chattoraj¹

Received: 25 October 2023 / Accepted: 9 July 2024
© Indian Society of Remote Sensing 2024

Abstract

In developing countries, exploration and exploitation of mineral resources help create the infrastructure that can sustain the population and economic growth. Remote sensing makes a brilliant tool to boost this growth. Hyperspectral Remote Sensing has been a key technology in mineral exploration and mapping for some time now. In this study, Airborne Visible InfraRed Imaging Spectrometer – Next Generation (AVIRIS-NG) data with the high spatial and spectral resolution was deployed to map the metasedimentary rocks in parts of the Bhukia region of Banswara district, Rajasthan. Similarly, PRecursores IperSpettrale della Missione Applicativa (PRISMA) data is also utilized to achieve a similar goal. The rock spectra obtained from both the surface reflectance hyperspectral datasets after applying the processing techniques were compared against the USGS spectral library and the field/ laboratory spectra to identify the diagnostic spectral features. The spectral Angle Mapper algorithm was applied to both datasets and detected limestone, dolomite, phyllite, and quartzite rocks. Furthermore, absorption band parameters were estimated and interpreted to corroborate the chemistry of the rock which helped in the identification of limestones based on Al^{3+}/Mg^{2+} content.

Keywords Mineral Exploration · AVIRIS-NG · PRISMA · Spectral Angle Mapper (SAM) · Absorption band Parameters

Introduction

For developing countries, exploration and exploitation of mineral resources play a major role in boosting their infrastructure and economic development. The mineral deposits are scattered homogeneously all over the Earth's surface as a result of magmatic and tectonic activities. So, exploring these mineral deposits or resources becomes paramount to facilitate and sustain the development of any developing nation. The primary goal of spectroscopy is to spectrally delineate and distinguish between various rocks and minerals using their diagnostic absorption features (Hunt, 1977), which are the result of interactions between the surface and incident electromagnetic radiation (Clark et al., 2003). The spectral reflectance or absorption features are produced by a variety of electronic processes, including charge transfer processes, crystal fields and vibrational atomic movements

(Clark, 1999). Mineral spatial mapping is facilitated by the unique combination of spatially contiguous spectra and spectrally contiguous images provided by hyperspectral sensors (Goetz et al., 1985). For target detection, imaging spectroscopy uses diagnostic absorption features from the reflectance spectra of rocks and minerals (Goetz et al., 1985; Clark, 1999; Clark et al., 2003). Subsequently, Airborne Visible/ Infrared Imaging Spectrometer (AVIRIS) was developed in 1987 by NASA at the Jet Propulsion Laboratory (JPL) which offers 224 bands with a spectral resolution of 10 nm from 400 to 2500 nm provided airborne platform for imaging spectrometry. The spatial distribution of spectrally distinct minerals that occur as primary rock-forming minerals, secondary alteration products, and weathered products was identified by Kruse et al. (1993) using AVIRIS data. Kruse et al. (2003) successfully compared the AVIRIS and Hyperion sensors to study the hyperspectral domain in the field of remote sensing broadly and concluded that the quality of data acquired by remote sensors depends on the signal-to-noise ratio (SNR) along with spectral and spatial resolution wherein AVIRIS performed comparatively better.

In 1998, Baugh et al., employed AVIRIS data to map the concentration of minerals (such as buddingtonite) with

✉ Richa Upadhyay Sharma
richa@iirs.gov.in; richaupadhyay00z@gmail.com

¹ Geosciences Department, Indian Institute of Remote Sensing, Dehradun, India

diagnostic absorption characteristics in hydrothermally altered volcanic rocks in the southern Cedar Mountains, Esmeralda County. In another study, Crosta et al., 1998 utilized AVIRIS data to examine the spectral angle mapper and Tricorder algorithm for mapping the kaolinite group of minerals and ferric oxides. Van der Meer (2004) derived absorption-band position, depth, and asymmetry from AVIRIS data using a linear interpolation technique in the Cuprite mining area Nevada, USA that is used to interpret the data in terms of the known alteration phases characterizing the area. Off late, AVIRIS was upgraded to AVIRIS-NG (Next Generation) which is a highly capable sensor consisting of 425 bands at a sampling interval of 5 nm in the 380–2510 nm spectral range. There have been several studies encompassing mineral and lithological mapping (Chabrilat et al., 2000; Kruse et al., 2002; Govil et al., 2018; Jain & Sharma, 2019; Kumar and Rajawat, 2020; Chatteraj et al., 2020). A comparative study using various classification techniques to map talc abundance and its spectral characteristics were studied using AVIRIS-NG data in Jahazpur Belt in Rajasthan (Bhadra et al., 2020). Tripathi and Govil (2019) evaluated AVIRIS-NG data to identify and map minerals in the Jahazpur region of Bhilwara district, Rajasthan. From AVIRIS-NG data, Bhattacharya et al., 2019 delineated minerals associated with ultramafic kimberlitic suite using relative band depth technique. Rani et al. (2020) demarcated metasedimentary rocks using the same technique in Banswara. Kokaly et al. (2017) used HyMap imaging spectrometer data to analyze white mica and elevated Cu values of the Orange Hill porphyry copper deposit in Orange Hill-Bond Creek, Alaska. Graham et al. (2018) applied HyMap hyperspectral RS data to map the distribution of the predominant alteration minerals in unmined porphyry Cu deposits in the eastern Alaska Range. Tan et al., 2020 proposed a band selection (BS) method for hyperspectral lithologic discrimination by utilizing two HIS datasets, i.e., the Cuprite, Nevada, USA, based on AVIRIS images and the Junggar, Xinjiang, China, based on Hyperion images. Adiri et al., 2020 utilized EO-1 Hyperion data fusion with Landsat 8 OLI and Sentinel-2 A in Moroccan Anti-Atlas for mapping copper mineralization. Guha et al., 2021 delineated the surface signatures associated with the base metal mineralization in the Pur-Banera area in the Bhilwara district, Rajasthan, India. Mondal et al., 2022 identified potential chromite exploration zones in Sittampundi District, Tamil Nadu by integrating AVIRIS-NG hyperspectral and ground geophysical data using support vector machines.

As for the evolution of space-borne hyperspectral imaging, a major thrust was provided by NASA's Hyperion sensor onboard EO-1 satellite which placed itself as the first widely used hyperspectral data source year 2000 onwards for land cover surface chemistry, after that in 2019 Italy's

ASI deployed the PRecursoRE IperSpettrale della Missione Applicativa (PRISMA), a medium spectral resolution hyperspectral imaging equipment, excluding in between contributions from sensors like HysIS, HysI etc. Tripathi and Garg (2020) utilized PRISMA data to study the spectral ability of the sensor in mineral identification and mapping. In another study, Bedini et al. (2020) evaluated PRISMA data for mineral detection and mapping at the alteration system of Cuprite, Nevada resulting in accurate detection of alteration minerals such as alunite, kaolinite, and illite/muscovite. Benhalouche et al. (2021) applied a linear NMF unmixing-based approach to PRISMA remote sensing hyperspectral data for detecting and mapping nine minerals in the Algerian Central Hoggar region. Bedini and Chen (2022) used the PRISMA hyperspectral imagery to characterize an extensive hydrothermal alteration system in the Kap Simpson igneous complex in central East Greenland. In the Bhilwara district in southern Rajasthan's Jahazpur town, Mishra et al. (2022) conducted a comparative study of aerial AVIRIS-NG and spaceborne PRISMA hyperspectral datasets for mapping hydrothermally changed minerals.

Synergy of AVIRIS-NG and PRISMA hyperspectral datasets, thus holds promise for its effective utilization in lithological discrimination and mapping in parts of the Bhukia region in the Banswara district of Rajasthan. Moreover, absorption-band parameters including the position, depth, and asymmetry of the absorption feature were analyzed using the linear interpolation method taking cues from hyperspectral laboratory reflectance data to evaluate the mineralogical variation.

Study Area

The study area forms the part of Banswara District of Rajasthan, located in Survey of India degree sheets 46E and I, with a latitude and longitude of 23°36'22.50"N and 74°15'0.42"E (Fig. 1). The area of interest lies 40–50 kms towards east from the Banswara town. The study area is located near and around the India Cements Ltd. factory in Nokla Village. It spans southwards from Partipura Mines of India Cements Ltd. to Umrai. The study area, stratigraphically, falls within the Lunavada Group of the Aravalli Supergroup consisting of phyllite, metagreywacke, mica schist, dolomite, dolomitic marble, and amphibole schists (after GSI, 2000). The study area comprises metasedimentary rocks of the Kalinjara Formation with dolomite, limestone, phyllite and quartzite. The rocks are highly weathered at places, having a greyish black appearance. The strike of the rocks in the area trends NW-SE with beds dipping up to 80°. The quartzite and dolomite/ limestone can be observed to form sporadic structural ridges.

Materials and Methodology

Materials

AVIRIS-NG data of Feb 3, 2016 was used for the study. AVIRIS-NG is a powerful sensor developed by JPL NASA with 425 bands at a sampling rate of 5 nm, operating in the 380–2510 nm spectral region. The spatial resolution is 4 m whilst radiometric resolution is 14 bits with SNR of >2000 @ 600 nm and >1000 @ 2200 nm). The AVIRIS-NG is a whisk-broom imaging spectrometer and the dataset used for processing is at surface L2 reflectance data. Two tiles of PRISMA data of March 3, 2021 and March 16, 2022 were used. PRISMA is a push-broom imaging spectrometer with a spatial resolution of 30 m and a sampling rate of 12 nm that can capture images in the spectral range of 400 to 2505 nm. It has a radiometric resolution of 12 bits. It includes 173 SWIR bands and 66 VNIR bands. The PRISMA dataset used for processing is L2D which is at surface geocoded reflectance data. It has a spectral and radiometric resolution of 30 m and 12 bits, respectively with SNR of 200 in the range 0.4–1.0 μm , 600 @ 0.65 μm , 200 in the range 1.0–1.75 μm , > 400 @ 1.55 μm , 100 in the range 1.95–2.35 μm , > 200 @ 2.1 μm . The ASD FieldSpec 4 Hi-Res spectroradiometer (field instrument) was used which has a spectrum in the range of 350–2500 nm at a sampling rate of 3 nm for VNIR and 10 nm for SWIR. District resource map (GSI, 1:25000 scale), geological map (GSI, 1:50000 scale), and a base map of the study area were used as ancillary data with ENVI 5.0 and QGIS and ArcGIS (©ESRI Ltd.) used as processing softwares.

Methodology

Prior to the processing of reflectance data from both the sensors, bands with poor information and the water absorption bands were selectively removed. The inherent dimensionality of the reflectance image data was determined using the Minimum Noise Fraction (MNF) transformation which also separates out input noise and lowers the computation for further processing. Next, the Pixel Purity Index (PPI) (Boardman, 1993), is used to locate the most spectrally pure pixels in the image. PPI was computed by repeatedly projecting n-dimensional scatterplots onto a random unit vector. Each projection's extreme pixels were recorded, along with the total number of times each pixel has been designated as extreme. The final endmembers selected from extreme or pure pixels were used as input for classification. The image was classified using spectral angle mapper (SAM). The algorithm calculates the degree of spectral similarity between two spectra by measuring the angle between the vectors in the n-dimensional space that represent the endmember

spectra. The spectral signatures of rock samples were collected from the field as well as in the laboratory using the ASD spectro-radiometer as mentioned in the above section. These spectra of rocks were compared with the USGS mineral spectral library to match the spectrally similar minerals. Similarly, selected endmembers extracted from the image were validated after being compared to field and laboratory spectra. Following this, absorption band parameters (depth, asymmetry, and position) were calculated using linear interpolation (Van Der Meer, F, 2004) which helps to evaluate the composition of the rock. The flow chart of methodology is given in Fig. 2 Further, gamma-ray spectroscopy was utilized to corroborate the composition of the rock samples. It is used in geochemical analysis to identify and quantify the gamma emitters present in a gamma source.

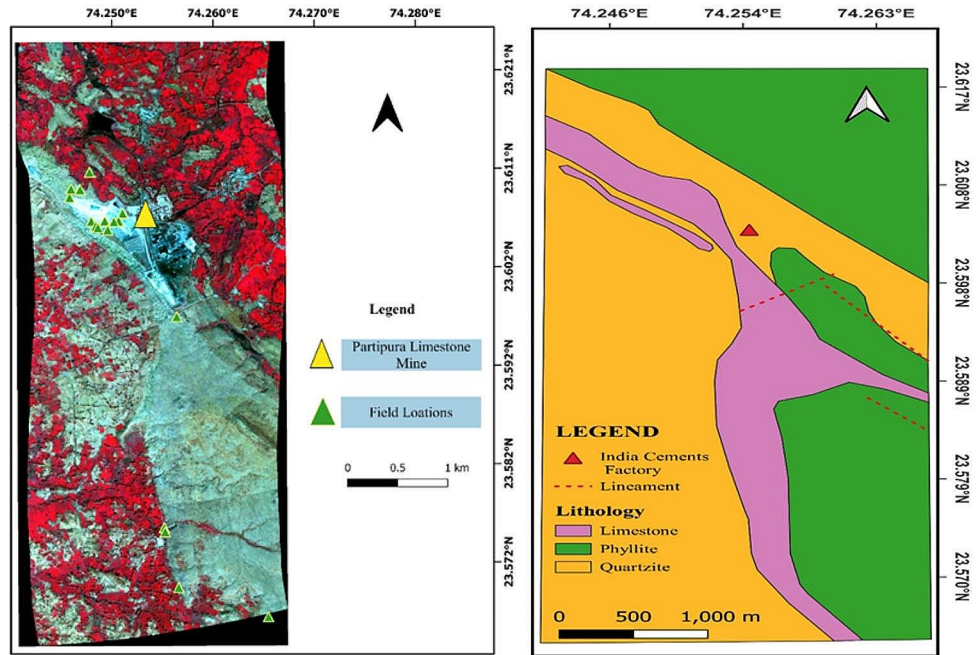
Results

The final outputs for the lithological discrimination of the study area are a direct outcome of compilation of datasets obtained through various techniques performed on hyperspectral data. A total of 366 bands out of 425 in AVIRIS-NG and 200 out of 234 bands in PRISMA were used for processing.

For the AVIRIS-NG dataset, a total of 15 bands out of 366 input bands and for PRISMA dataset, a total of 14 bands out of 200 input bands were selected based on eigenvalues using MNF technique. The highest eigenvalues for AVIRIS-NG and PRISMA are 153.75 and 141.71 respectively. For AVIRIS-NG, 15 MNF bands were entered as input for which threshold was kept at 1 and an iteration at 30,000 for pixel purity index (PPI) and for PRISMA, 14 MNF bands were entered with threshold 2.0 and an iteration at 5000. The classes or endmembers selected were confirmed after comparing against field and lab spectra as well as the USGS spectral library with associated overall scores indicative of the spectral match (shown in Table 1). In the case of AVIRIS-NG, there were four lithological classes identified viz. limestone Types 1 and 2, phyllite, and quartzite (impure). Quartz, kaolinite, montmorillonite, chlorite, and type 1 and type 2 calcite are found to be the constituent mineral species for the four detected lithological groups. While phyllite was recognized due to the presence of kaolinite, montmorillonite, and chlorite. Limestone types 1 and 2 are represented by different calcite species based on spectral characteristics. Impure quartzite was identified owing to the presence kaolinite and quartz (with Al replacing Si in the tetrahedral site).

For PRISMA, two lithological classes were identified viz. Dolomite and Phyllite. They were confirmed by identifying

Fig. 1 Location Map of the study area (left) in an AVIRIS-NG (98,56,36) and Geological Map (right) of study area (after GSI, 2000)



the mineral classes like dolomite (Table 2) (for dolomite/dolostone); kaolinite and phlogopite for phyllite.

The depth, asymmetry, and wavelength position of the absorption band were calculated for laboratory samples of all the four classes identified (Table 3; Fig. 3). The depth,

asymmetry, and wavelength position of the absorption band were calculated for Mg-OH dip in limestone type 1 and 2 laboratory samples are shown in Table 4. The complementary analysis of gamma-ray spectroscopy provided the results for limestone as given in Table 5.

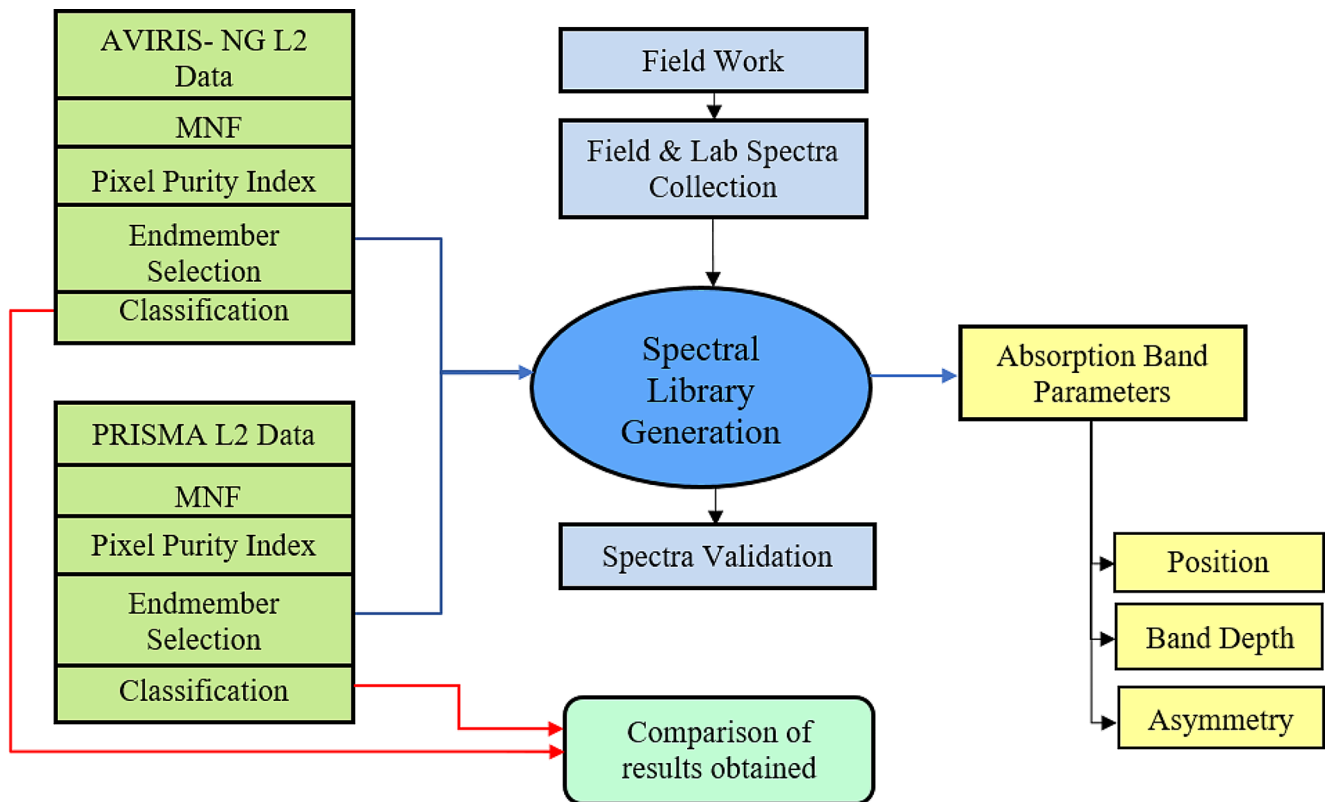


Fig. 2 Flow chart of methodology

Table 1 Endmembers from AVIRIS-NG with their associated overall score

Rock Name	Mineral Name	Score
Limestone Type 1	Calcite type 1	0.764
Limestone Type 2	Calcite type 2	0.755
Phyllite	Kaomectite	0.759
	Montmorillonite	0.757
	Chlorite	0.704
Quartzite	Quartz	0.728
	Kaomectite	0.719

Table 2 Endmembers identified from PRISMA with their associated overall score

Rock Name	Mineral Name	Score
Dolomite	Dolomite	0.536
Phyllite	Kaomectite	0.577
	Phlogopite	0.535

Table 3 Absorption band parameters for lab samples

Rock Type	Position (μm)	Depth	Asymmetry
Limestone Type 1	2.327	0.297	0.095
Limestone Type 2	2.321	0.220	0.121
Phyllite	2.330	0.170	0.006
Quartzite	2.214	0.029	0.012

Discussion

The minerals for both the datasets were classified (Fig. 4) using spectral angle mapper (SAM), which, as well, include only one linear anthropogenic feature in the central part of Fig. 4b, owing to over classification and special resolution of PRISMA data, preferably to be ignored. The AVIRIS-NG differentiated the lithology into four classes (Fig. 4, 5 and 6) namely, limestone type 1 and 2, phyllite and impure quartzite. The quartzite is manifested by the presence of

Table 4 Absorption band parameters for limestone type 1 & 2 Mg-O/OH absorption dip

Rock Type	Position (μm)	Depth	Asymmetry
Limestone Type 1	2.204	0.0956	0.0013
Limestone Type 2	2.219	0.1854	0.031

Table 5 Gamma-ray analysis for limestone type I and 2

Composition	Lime stone type-I Quantity (%)	Lime stone type-II Quantity (%)
CaO	48.786	44.069
Al ₂ O ₃	0.507	1.108
Fe ₂ O ₃	0.424	0.655
MgO	1.330	1.281
SiO ₂	9.126	16.167

inter-crystalline Al which causes an absorption dip at the wavelength of 2204 nm which is rendered due to the impurity of the rock. This inter-crystalline Al is confirmed by the presence of kao-smectite.

The PRISMA also classified dolomite and phyllite phases (Fig. 7) with phyllite being indicated by phlogopite and kaomectite. The image and the USGS library spectral plot of kaomectite demonstrates a doublet induced by the Al-OH bond situated roughly at 2160 and 2204 nm and a vibrational absorption characteristic caused by OH at about 1450 nm. It should be noted that kaolinite contains less water than other minerals causing the peak at about 1900 nm to be highly diminished. The spectral characteristics of Montmorillonite is very much similar to that of Kaolinite. Montmorillonite is extremely distinctive among the clay minerals in terms of its absorption depth at 1395 and 1415 nm owing to OH overtones and 2163 and 2209 nm for the combination of AL-OH bend and OH stretch. The stronger absorption at 1.9 to 2 μm also suggests that water

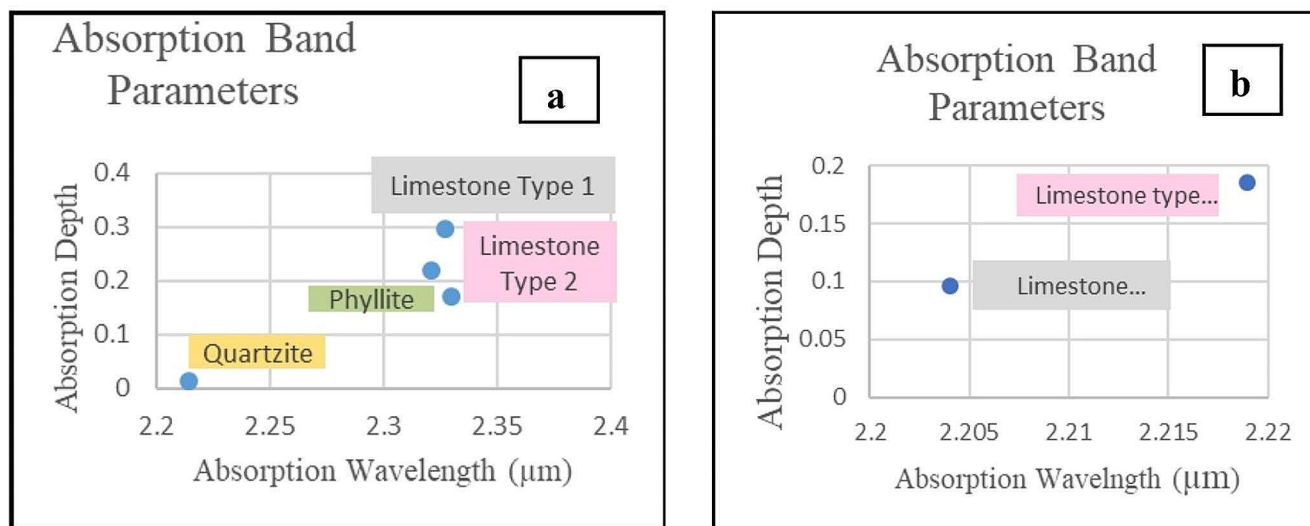


Fig. 3 Absorption band parameters plot for (a) lab samples and (b) limestone type 1 & 2 Mg-O/OH absorption dip

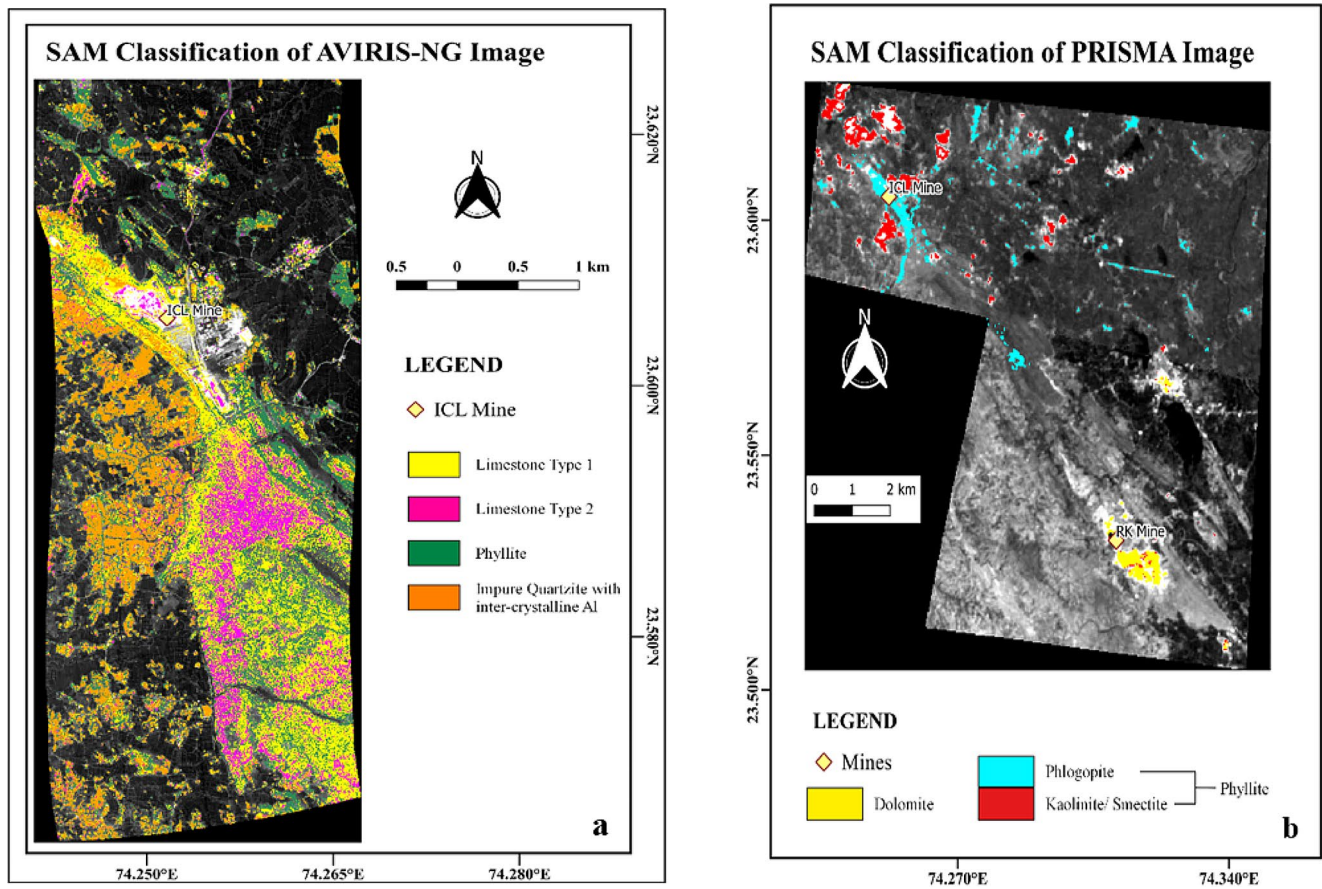


Fig. 4 SAM Classified image for (a) AVIRIS-NG derived classes and (b) PRISMA derived classes

predominates over hydroxyl ion in the mineral. The conspicuous absorption caused by the combination of metal Mg-OH bend and OH stretch at 2339, which is seen in both image-derived and lab spectra, can also be noted. Similar to the montmorillonite, the Mg-OH bond and OH stretch is also responsible for the diagnostic absorption feature of phlogopite at 2320 nm and 2378 nm. Another mineral, chlorite (clinocllore) being Mg^{2+} rich with the Mg-OH bond and OH stretch indicates diagnostic dip at 2329 nm. It also shows slight dips at 900 nm and around 1400 nm. The dolomite shows a diagnostic dip of 2320 nm in the PRISMA

dataset. The carbonates causing the absorption dip at 2334 to 2339 nm indicated in the AVIRIS-NG represents the calcite mineral which is further classified into two types viz. type 1 and 2 because of their dip at 2204 nm to 2219 nm owing to the Mg-O/ OH bond. The calcite type 1 and type 2 are categorized on the basis of absorption or band depth (BD) at the 2204 nm in limestone 1 and 2. Type 2 shows absorption depth of 0.1854 compared to 0.0956 of type 1. Type 2 limestone is also found to be more silica rich than type 1. The BD of limestone type 2 (Si-rich) is more than limestone type 1 (Si-poor) at 2204 to 2219 nm signifying

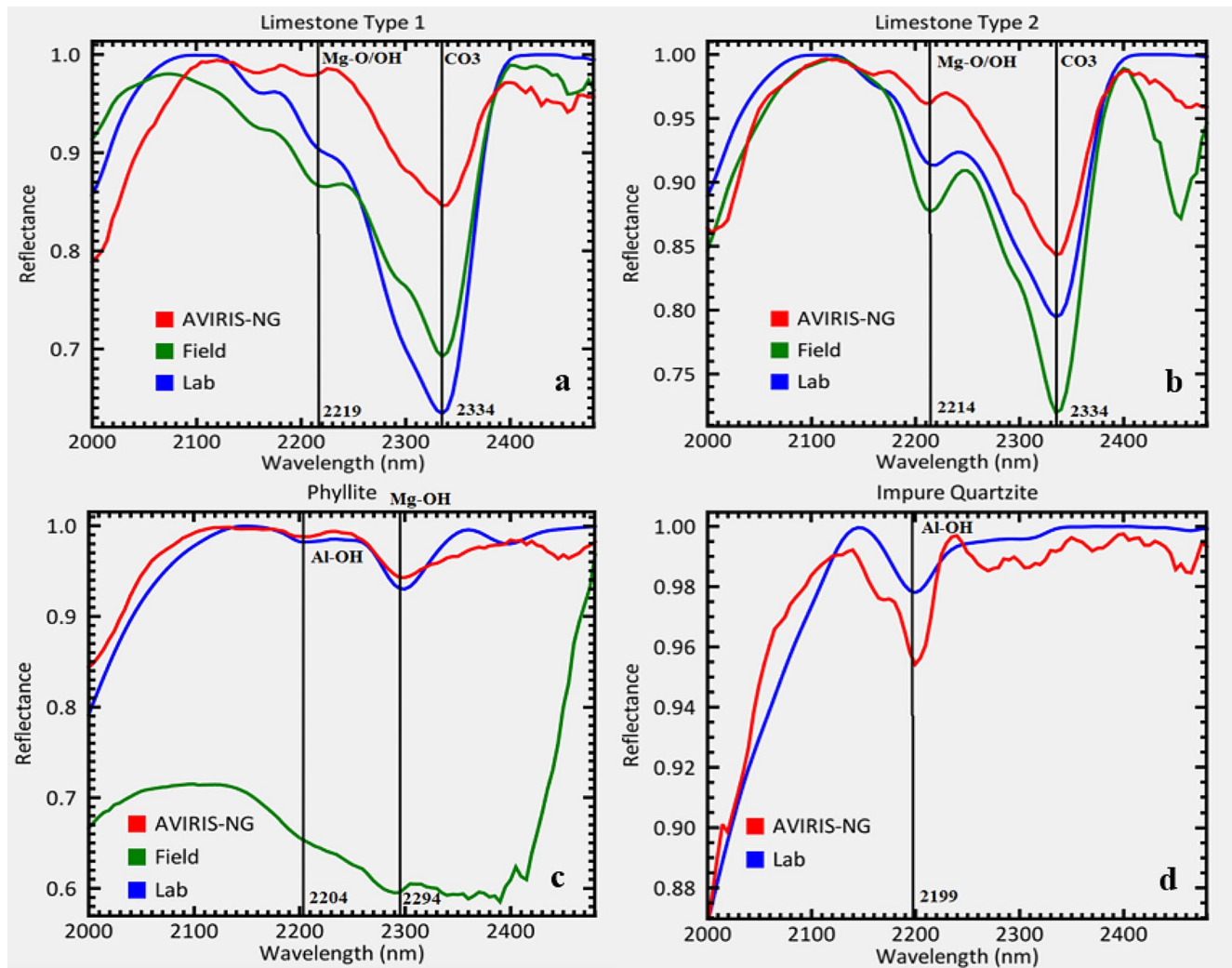


Fig. 5 AVIRIS-NG resampled laboratory (Blue) and field spectra (Green) and corresponding image spectra (Red) of (a) limestone type 1 (b) limestone type 2 (c) phyllite and (d) quartzite (impure)

concomitant variation in inter-crystalline $\text{Al}^{3+} / \text{Mg}^{2+}$ ratio, rendering difference in color (slight pink as observed in the field), as also confirmed by gamma ray spectroscopy analysis. The $\text{Al}^{3+} / \text{Mg}^{2+}$ ratio for type 2 is 0.92 whereas for type 1 is 0.38, revealing a significant difference in composition. These image spectra were compared against field/ lab and the USGS spectral library to match the absorption behavior. The absorption wavelength (position) of limestone (both types) remained similar, so did their BD with a minor difference. This is because of the insignificant change in CaO content which is confirmed by gamma spectroscopy. Asymmetry is slightly positive which indicates visible skewness

towards longer wavelength. Phyllite, 2330 nm and impure quartzite 2214 nm show considerable difference in their position whilst BD remains 0.17 and 0.029, respectively. They are both skewed towards the longer wavelengths indicating the predominance of Ca content. The phyllite rock also shows a small positive value i.e. skewing towards longer wavelengths. The presence of montmorillonite, chlorite and kaolinite in the phyllite has near zero to small positive asymmetry. Thus, the important rock-forming minerals including their sub-types in the study area were differentiated based upon the analysis of absorption band parameters.

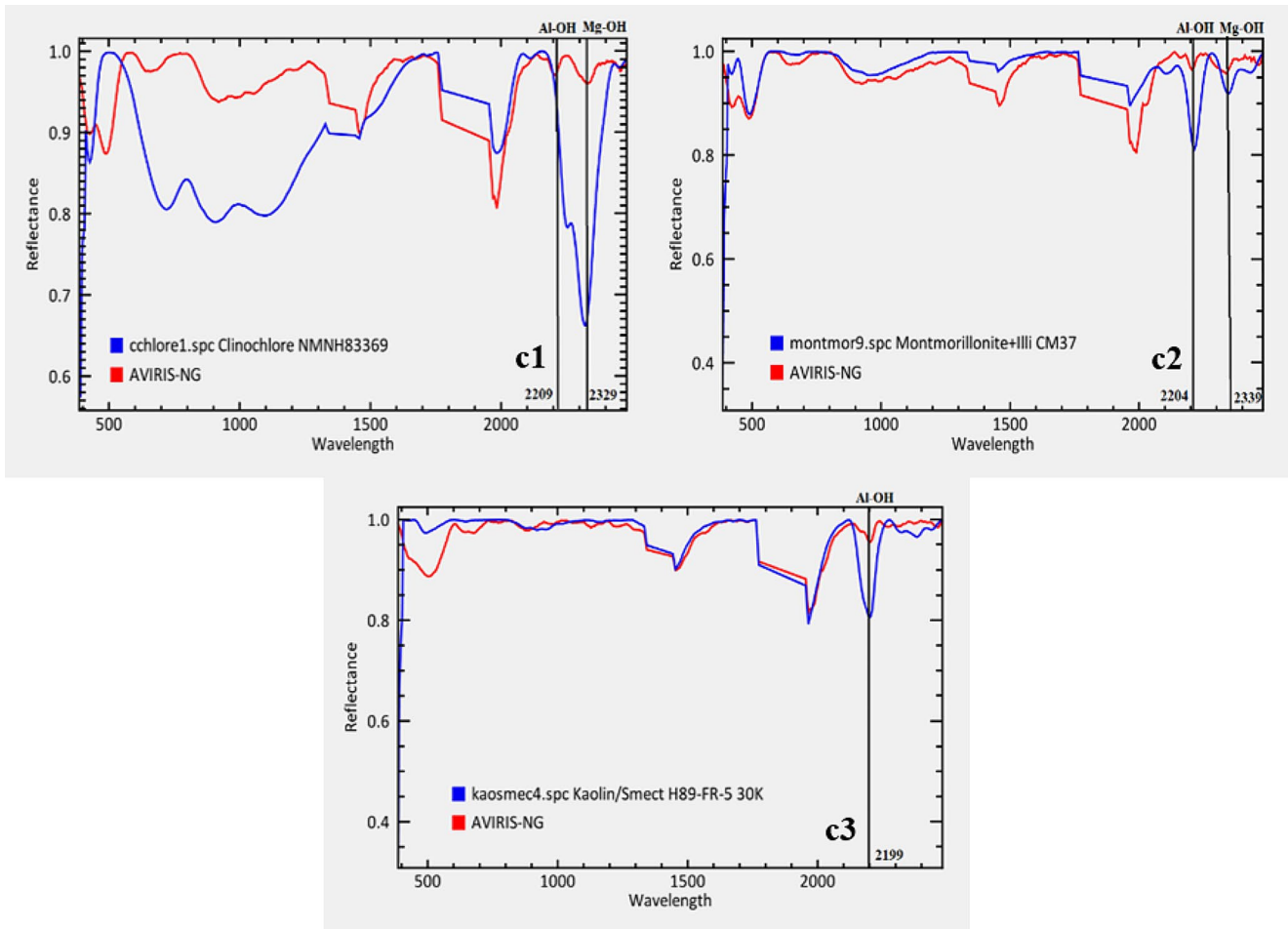


Fig. 6 AVIRIS-NG image spectra (Red) and USGS image spectra (Blue) of **(c1)** Chlorite/Clinochlore **(c2)** Montmorillonite and **(c3)** Kaosmectite for phyllite

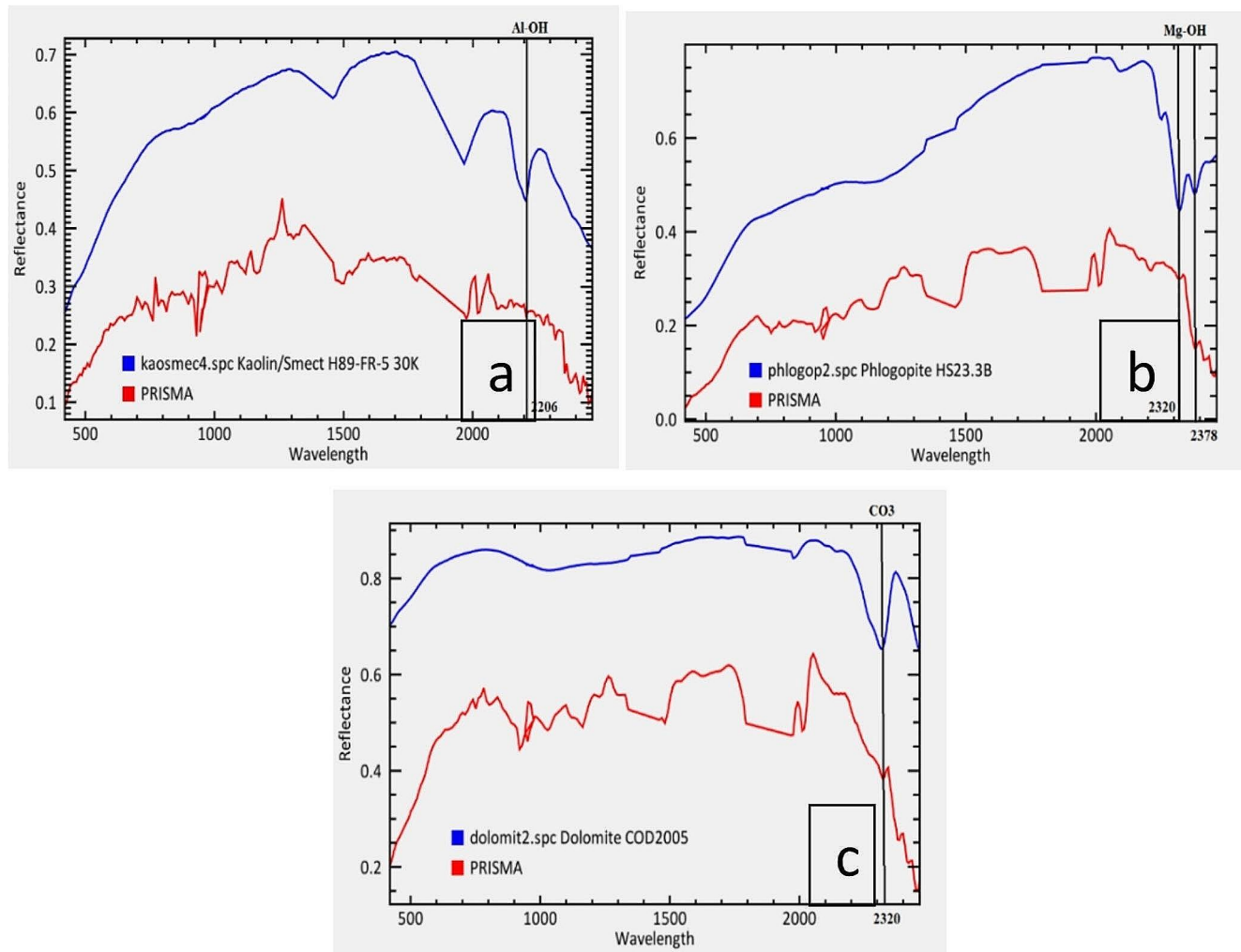


Fig. 7 PRISMA spectra (Red) and USGS image spectra (Blue) of (a) kaolinite (b) phlogopite for (phyllite) and (c) dolomite

Conclusions

The AVIRIS-NG provided more accurate spectral signatures owing to its high spatial resolution and high signal to noise ratio than the PRISMA. Although, AVIRIS-NG has limited availability and coverage whilst PRISMA has more coverage and availability, albeit. AVIRIS-NG data revealed calcite, kaolinite, montmorillonite, chlorite, and quartz whereas PRISMA identified kaolinite, phlogopite and dolomite. The accuracy of minerals found in PRISMA is comparatively less with respect to the field/ lab data and AVIRIS-NG. Absorption band parameters not only revealed the presence of major mineral phases, but also provided inputs on the compositional change in sub-variants (lime stone type 1 and 2) owing to surface weathering and impurities. This study throws light on how the synergetic use of available hyperspectral data (air and space-borne) can be utilized in better characterization and identification of important minerals, thereby, aiding mineral exploration.

Acknowledgements The authors would like to thank IIRS-ISRO for their infrastructural support throughout the research. We are also grateful to the authorities of India Cements Ltd., Banswara, Rajasthan, for their support during field data collection and for providing us with the gamma-ray spectroscopy data.

Author contribution AR: Data collection, processing, result analysis, article drafting. RU: Conceptualization, Data collection, processing, article editing, communication. SLC: Conceptualization, Article evolution.

Funding The authors would like to thank IIRS-ISRO for their funding support throughout the research.

Declarations

Conflict of interest The authors declare that there is no conflict of interest.

References

- Adiri, Z., El Harti, A., Jellouli, A., Maacha, L., Azmi, M., Zouhair, M., & Bachaoui, E. M. (2020). Mapping copper mineralization using EO-1 Hyperion data fusion with landsat 8 OLI and Sentinel-2A in Moroccan Anti-atlas. *Geocarto International*, 35(7), 781–800. (visited on 10-06-2022) <https://www.asdi.com/products-and-services/fieldspec-spectroradiometers>.
- ASI (2022). <https://prisma.asi.it/>.
- Baugh, W. M., Kruse, F. A., & Atkinson Jr, W. W. (1998). Quantitative geochemical mapping of ammonium minerals in the southern Cedar Mountains, Nevada, using the Airborne Visible/Infrared imaging spectrometer (AVIRIS). *Remote Sensing Environ*, 65(3), 292–308.
- Bedini, E., & Chen, J. (2020). Application of PRISMA satellite hyperspectral imagery to mineral alteration mapping at Cuprite, Nevada, USA. *Journal of Hyperspectral Remote Sensing v*, 10(2), 87–94.
- Bedini, E., & Chen, J. (2022). Prospection for economic mineralization using PRISMA satellite hyperspectral remote sensing imagery: An example from central East Greenland. *Journal of Hyperspectral Remote Sensing*, v12, 124–130.
- Benhalouche, F. Z., Benabbou, O., Kebir, L. W., Bennia, A., Karoui, M. S., & Deville, Y. (2021, July). An Informed NMF-Based Unmixing Approach for Mineral Detection and Mapping in the Algerian Central Hoggar Using PRISMA Remote Sensing Hyperspectral Data. In *2021 IEEE International Geoscience and Remote Sensing Symposium IGARSS* (pp. 1863–1866). IEEE.
- Bhadra, B., Pathak, S., Nanda, D., Gupta, A., & Sitiraju, S. (2020). Spectral characteristics of talc and mineral abundance mapping in the Jahazpur Belt of Rajasthan, India using AVIRIS-NG Data. *International Journal of Remote Sensing*, 41, 8754–8774. <https://doi.org/10.1080/01431161.2020.1783710>
- Bhattacharya, S., Kumar, H., Guha, A., Dagar, A. K., Pathak, S., Rani, K., & Rajawat, A. S. (2019). Potential of airborne hyperspectral data for geo-exploration over parts of different geological/metallogenic provinces in India based on AVIRIS-NG observations. *Current Science*, 116(7), 1143–1156.
- Boardman, J. W. (1993, October). Automating spectral unmixing of AVIRIS data using convex geometry concepts. *JPL, Summaries of the 4th annual JPL Airborne Geoscience Workshop* (Vol. 1). AVIRIS Workshop.
- Chabrilat, S., Pinet, P. C., Ceuleneer, G., Johnson, P. E., & Mustard, J. F. (2000). Ronda Peridotite massif: Methodology for its geological mapping and lithological discrimination from airborne hyperspectral data. *International Journal of Remote Sensing*, 21(12), 2363–2388.
- Chattoraj, S. L., Sharma, R. U., Kumar, C., & Sengar, V. (2020). Identification and characterization of hydrothermally altered minerals using surface and space-based reflectance spectroscopy, in parts of south-eastern Rajasthan, India. *SN Applied Sciences*, 2(4), 1–9.
- Clark, R. N. (1999). Spectroscopy of rocks and minerals, and principles of spectroscopy. *Man Remote Sens*, 3(3–58), 2–2.
- Clark, R. N., Swayze, G. A., Livo, K. E., Kokaly, R. F., Sutley, S. J., Dalton, J. B., McDougal, R. R., & Gent, C. A. (2003). Imaging spectroscopy: Earth and planetary remote sensing with the USGS tetracorder and expert systems. *Jour Geophys Res : Planets*, 108(E12).
- Crosta, A. P., Sabine, C., & Taranik, J. V. (1998). Hydrothermal alteration mapping at Bodie, California, using AVIRIS hyperspectral data. *Remote Sensing Environ*, 65(3), 309–319.
- Geological Survey of India (2000). District Resources of Banswara, Rajasthan.
- Goetz, A. F., Vane, G., Solomon, J. E., & Rock, B. N. (1985). Imaging spectrometry for earth remote sensing. *Science*, 228(4704), 1147–1153.
- Govil, H., Tripathi, M. K., Diwan, P., & Guha, S., and Monika (2018). Identification of Iron Oxides minerals in Western Jahajpur region, India using AVIRIS-NG hyperspectral remote sensing. *Int Arch Photogramm Remote Sens Spatial Inf Sci*, XLII-5, 233–237. <https://doi.org/10.5194/isprs-archives-XLII-5-233-2018>.
- Graham, G. E., Kokaly, R. F., Kelley, K. D., Hoefen, T. M., Johnson, M. R., & Hubbard, B. E. (2018). Application of imaging spectroscopy for mineral exploration in Alaska: A study over porphyry Cu deposits in the eastern Alaska Range. *Economic Geology*, 113(2), 489–510.
- Guha, A., Kumar Ghosh, U., Sinha, J., Pour, A. B., Bhaisal, R., Chatterjee, S., & Rao, P. V. (2021). Potentials of airborne hyperspectral AVIRIS-NG data in the exploration of base metal deposit—a study in the parts of Bhilwara, Rajasthan. *Remote Sensing*, 13(11), 2101.
- Hunt, G. R. (1977). Spectral signatures of particulate minerals in the visible and near-infrared. *Geophysics*, 42, 501–513.
- Jain, R., & Sharma, R. U. (2019). Airborne hyperspectral data for mineral mapping in Southeastern Rajasthan, India. *International Journal of Applied Earth Observation and Geoinformation*, 81, 137–145.
- Kokaly, R., Graham, G. E., Hoefen, T. M., Kelley, K. D., Johnson, M. R., Hubbard, B. E., & Prakash, A. (2017). Multiscale hyperspectral imaging of the Orange Hill Porphyry Copper Deposit, Alaska, USA, with laboratory-, field-, and aircraft-based imaging spectrometers. In *Proc. Explor* (Vol. 17, pp. 923–943).
- Kruse, F. A., Lefkoff, A. B., & Dietz, J. B. (1993). Expert system-based mineral mapping in northern Death Valley, California/Nevada, using the airborne visible/infrared imaging spectrometer (AVIRIS). *Remote Sensing Environ* v, 44(2–3), 309–336.
- Kruse, F. A., Perry, S. L., & Caballero, A. (2002). Integrated multispectral and hyperspectral mineral mapping, Los Menucos, Rio Negro, Argentina, Part II: EO-1 Hyperion/AVIRIS comparisons and Landsat TM/ASTER extensions. In: Proc. 11th JPL Airborne Geoscience Workshop. Jet Propulsion Laboratory, Pasadena, California.
- Kruse, F. A., Boardman, J. W., & Huntington, J. F. (2003). Comparison of airborne hyperspectral data and EO-1 Hyperion for mineral mapping. *IEEE Trans Geoscience and Remote Sensing*, 41(6), 1388–1400.
- Kumar, H., & Rajawat, A. S. (2020). Aqueous alteration mapping in Rishabdev ultramafic complex using imaging spectroscopy. *International Journal of Applied Earth Observation and Geoinformation*, 88, 102084.
- Mishra, G., Govil, H., Guha, A., Kumar, H., Kumar, S., & Mukherjee, S. (2022). Comparative evaluation of airborne AVIRIS-NG and spaceborne PRISMA hyperspectral data in identification and mapping of altered/weathered minerals in Jahazpur, Rajasthan. *Advances in Space Research*.
- Mondal, S., Guha, A., & Pal, S. K. (2022). Support vector machine-based integration of AVIRIS NG hyperspectral and ground geophysical data for identifying potential zones for chromite exploration—A study in Tamil Nadu, India. *Advances in Space Research*.
- NASA (2022). <https://aviris-ng.jpl.nasa.gov/data.html>.
- Rani, K., Guha, A., Kumar, K. V., Bhattacharya, B. K., & Pradeep, B. (2020). Potential use of airborne hyperspectral AVIRIS-NG data for mapping proterozoic metasediments in Banswara, India. *Journal of the Geological Society of India*, 95(2), 152–158.
- Tan, Y., Lu, L., Bruzzone, L., Guan, R., Chang, Z., & Yang, C. (2020). Hyperspectral band selection for lithologic discrimination and

geological mapping. *IEEE Journal of Selected Topics in Applied Earth Observations and Remote Sensing*, 13, 471–486.

Tripathi, P., & Garg, R. D. (2020). First impressions from the PRISMA hyperspectral mission. *Current Science (00113891)*, 119(8).

Tripathi, M. K., & Govil, H. (2019). Evaluation of AVIRIS-NG hyperspectral images for mineral identification and mapping. *Heliyon*, 5(11), e02931.

Van Der Meer, F. (2004). Analysis of spectral absorption features in hyperspectral imagery. *International Journal of Applied Earth Observation and Geoinformation*, 5(1), 55–68.

Publisher's Note Springer Nature remains neutral with regard to jurisdictional claims in published maps and institutional affiliations.

Springer Nature or its licensor (e.g. a society or other partner) holds exclusive rights to this article under a publishing agreement with the author(s) or other rightsholder(s); author self-archiving of the accepted manuscript version of this article is solely governed by the terms of such publishing agreement and applicable law.